Experimental Research on Anti-slip Performance of Cables at the Saddle of Partially Cable-stayed Bridge

Hailin Liu[1,a], Peng Wang[2,3,b*], Yun Huang[1,c], Cheng Huang[1,d], Junliang Zhu[2,3,e]

[1]Guangxi Road Construction Engineering Group Co., Ltd., 1 Yongwu Road, Xingning District, Nanning, Guangxi, China
[2]China Merchants Chongqing Transportation Research & Design Institute Co. LTD, 33 Xuefu Avenue, Nanan District, Chongqing, China
[3]National Key Laboratory for Bridge Engineering Safety and Resilience, 33 Xuefu Avenue, Nanan District, Chongqing, China

[a]1049731031@qq.com,[b*]wangpeng@cmhk.com,[c]54381689@qq.com
[d]2585936256@qq.com,[e]806420430@qq.com.

Abstract: To address the issue of cable anti-slip at the saddle of pre-stressed concrete partially cable-stayed bridges, typical cables were selected and a full-scale model of the bridge tower segment and reaction beam combination was designed and constructed to conduct experiments on cable slippage resistance of the multi-tube bundled saddles. Simulating the unbalanced cable forces generated by operational loads during the service period, the displacement and cable forces on both sides of the saddle were tested under low-cycle repeated loads to study the slippage resistance performance and cable force transmission rate through the saddle. The reverse slippage resistance capacity was also studied by swapping the active and passive ends. The ultimate slippage bearing capacity of the saddle was studied by providing maximum tension at the active end of the cable. The research results show that under the action of unbalanced tension in dead load and 1x, 1.4x, and 2.5x live loads, the cable displacement at the saddle end mainly changes due to the elongation of the prestressed steel strands, and there is no sudden increase in cable displacement indicating slippage failure. The measured cable force transfer rate from the active end to the passive end is only a maximum of 0.3%. The slippage resistance performance of the saddle is reliable under reverse loading conditions. When the test device can exert a maximum cable force of 7200kN and a cable force difference of 2500kN, the anchor system of the saddle still has reliable slippage resistance capacity. The experiment reveals the slippage resistance performance of the saddle anchor system and verifies its reliability.

Keywords: partially cable-stayed bridge, full-scale model experiment, multi-tube bundled saddle, Shear key anti-slip anchoring device, anti-slip performance.

P. Xiang et al. (eds.), *Proceedings of the 2023 5th International Conference on Hydraulic, Civil and Construction Engineering (HCCE 2023)*, Atlantis Highlights in Engineering 26,
https://doi.org/10.2991/978-94-6463-398-6_33

1 Introduction

The cable saddle is an important structural component of partially cable-stayed bridges. The cables span the towers through the saddle and are anchored on the girder using saddles as the upper support points[1-2]. When there is a significant difference in tension between the cables on both sides of the tower, it might cause the cables to slip on the curved saddles, which poses a risk to the bridge. Scaled and full-scale model tests on adhesive anchorage cable saddles and strand anchorage cable saddles have also been conducted domestically to study their stress characteristics, friction coefficient, saddle load-bearing performance, and slip resistance[3-8]. In recent years, researchers have started to study some new type of strand anchorage cable saddle, such as conducting static load tests on a full-scale model of the 31-tube bundled saddle[9-10] and tests on diamond-shaped multi-tube saddle[11]. The multi-tube bundled saddle is becoming a general structural form in partially cable-stayed bridges[12-16], but related research is still insufficient, especially for large-scale cables and their saddle anchorage reliability[17].

2 Project Background

The Peisen Liu River Bridge is a (145+280+145)m prestressed concrete girder partially cable-stayed bridge, as shown in Figure 1. The bridge deck width is 29m, the main girder adopts variable-section box, which consists of three chambers. The cable towers are located within the central median, with a height of 50m. The tower is 3m wide in the transverse direction of the bridge, and 8m at the base and 6m at the top in the longitude direction. The bridge employs a pier-beam fixed system. The entire bridge is equipped with 46 pairs of stayed cables of 55Φs15.2mm steel strands. They pass through the towers by 55-tube bundled saddles equipped with anti-slip anchorage devices. The two ends of the cables are anchored in the top slab of the box girder. The bridge structure is complex, with extremely high safety requirements. The reliability of the shear key anti-slip anchorage devices of the saddles are critical. Due to the lack of relevant research, it is necessary to conduct experiments to study their anti-slip properties and anchorage reliability.

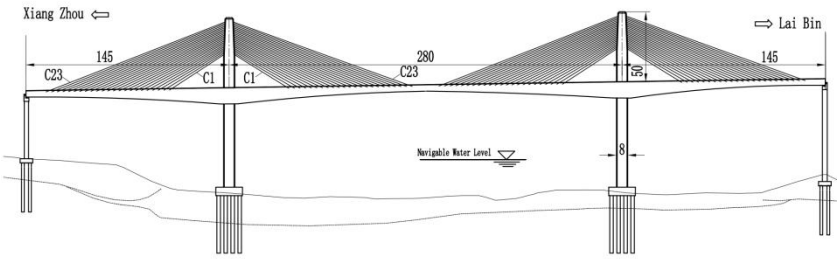

Fig. 1. Layout of Peisen Liu River Bridge

3 Design and fabrication of the anti-slip test model

A full-scale model of the cable tower segment was designed and constructed to conduct anti-slip experiments.

The experimental model consists of three parts: the reinforced concrete reaction beam, the tower segment and cables systems. The tower segment selected the representative C1 and C23 cables from the actual bridge as the research object, as shown in Figure 1. The scale of the tower model is 1:1 compared to the actual bridge, and it follows the principles of similarity in geometry, physics, and boundary conditions during the design and production. The cables C1 and C23 are designed according to the original design, and the radii of the cable saddle are 4m and 5m, respectively. The inclinations of the cables on both sides of the tower are shown in Figure 2(a). The longitudinal length of the reaction beam is 19.8m, the transverse width is 6m, and the height is 4.8m, constructed with a T-shaped section. Different angle concrete tooth blocks are designed for cable anchorage at the ends of the beam. The tower has a longitudinal length of 8m, a transverse width of 3m, and a height of 4.8m. Slip resistance tests on two different angled cables were conducted on the same model, which is the world-first in terms of scale. The completed model structure design and production are shown in Figure 2.

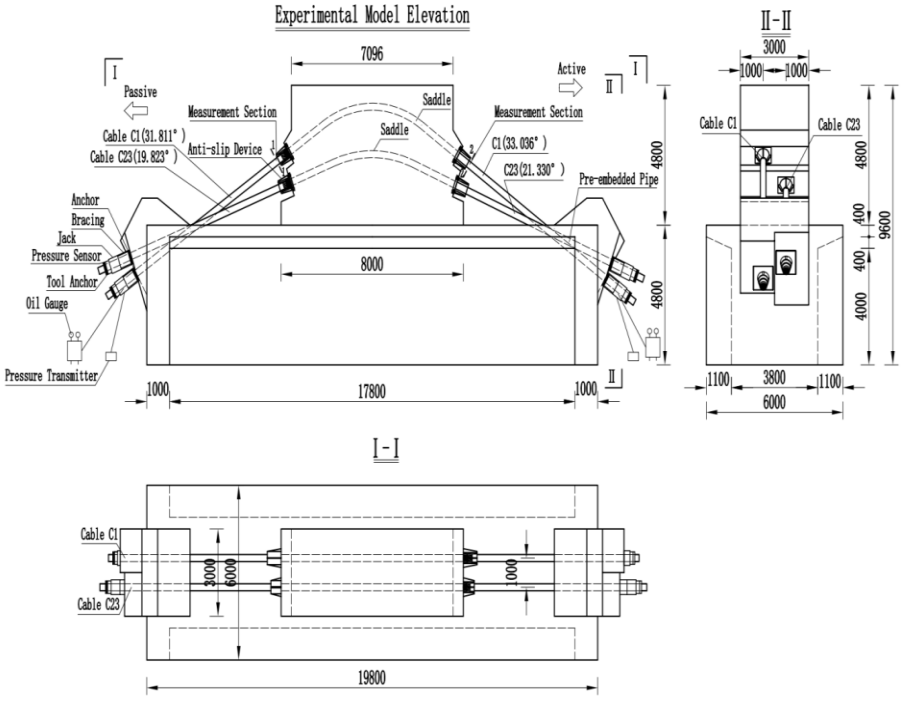

(a) Experimental model design

(b) Photo of the experimental model

Fig. 2. Experimental model

The anti-slip anchoring device, based on multi-tube bundled saddle, is composed of anti-slip keys that are extruded and fixed onto steel strands, isolation blocks, locking bolt and anchorage sleeve. A strands with an anti-slip key pass through a tube of the saddle. One end of the anti-slip key is supported on the end face of the saddle anchor plate, while the other end abuts against the end face of the subsequently installed anti-slip isolation block. The other end of the isolation block is in contact with the locking bolt that is tightened inside the anchoring sleeve finally. One end of the anti-slip key is restrained by the saddle anchor plate, while the other end is restrained by the isolation block, thereby achieving the effect of restricting bi-directional sliding of the steel strand. This is illustrated in Figure 3.

Fig. 3. The relationship between anti-slip key and insert of saddle

4 Experimental Plan and Procedure

4.1 Research Highlights

The key research points of the experiment include: Anti-slip performance of the anchoring device of the saddle, Reverse anti-slip capability, Cable force transmission rate, ultimate anti-slip bearing capacity.

4.2 Experimental Loading Process

The designed initial cable forces for C23 and C1 cables are 5500kN and 4700kN, respectively. According to the structural analysis, the unbalanced cable forces on the two sides of the saddle are 600kN and 550kN due to dead load at finished bridge state, and the most unfavorable unbalanced cable forces due to live loads are 350kN and 200kN for C23 and C1 cables respectively.

In the experiment, the anti-slip device is only installed on the left side of the cable tower, so the right side is considered as the active end while the left side is the passive end, as shown in Figure 2.

The main steps of the experiment are as follows:

- Test preparation

After installing the test cables, single steel strands are pre-tensioned. Gradual loading is performed at the active end and the passive end alternatively to reach the initial cable forces. Finally the unbalanced cable forces from the dead load for the active end are then added.

- Low-cycle cyclic loading process

Low-cycle cyclic loading test for unbalanced cable forces in C23 and C1 cables: The passive end cable forces are kept constant, and three low-cycle cyclic loading stages are added at the active end. Each stage consists of 10 cycles, with loading values of 1.0, 1.4, and 2.5 times the unbalanced cable forces due to live loads. It is about 5 minute a cycle.

- Reverse anti-slip capability loading

The active end cable force of C1 is firstly unloaded to the initial balanced cable force of 4700kN, then making it as the passive end. The original passive end becomes the active end, and it is loaded to 6000kN. Then, it is unloaded to 5250kN, followed by loading to 5750kN and unloading to 5250kN. This cycle is repeated 3 times to test the reverse anti-slip capability of the anchoring device.

- Ultimate anti-slip bearing capacity loading

The original passive end is unloaded to 4700kN and kept constant still as the passive end, while the original active end is loaded to 7200kN. Finally, a gradual unloading process is conducted. The main loading process of the experiment is shown in Figure 4.

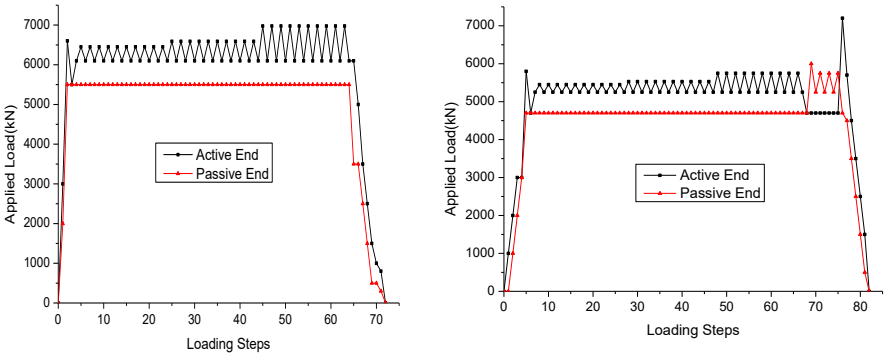

(a)Cable C23 loading (b) Cable C1 loading

Fig. 4. Test loading process

4.3 Test and Measurement

4.3.1.Cable Force Testing.

The cable forces are measured using pressure sensor installed between the jack and the anchor tool. A calibrated hydraulic pressure gauge and a digital pressure transmitter are used to collect the data, as shown in Figure 2, to ensure the reliability of the test data.

4.3.2.Cable Slip Testing.

Cable slip is measured using displacement gauges. Each cable test section is located near the saddle, as shown in Figure 2, marked as sections 1-1 and 2-2. Along the cable perimeter, three steel strands are selected on the upper, outer, and lower sides. Each cable has a total of 6 measurement points beside the saddle. The displacements of the cable are measured during the loading process. The arrangement of the displacement gauge at the measurement points is shown in Figure 5.

(a) Displacement measurement points layout (b) Installation of displacement sensors

Fig. 5. Displacement measurement points of cable at the end of saddle

4.4 Test Results Analysis

4.4.1.Calculation Method for Cable Elongation.

The saddle consists of three parts: a straight line segment, a circular arc segment, and another straight line segment, the two straight lines are tangent to the circular arc segment. During operation of the bridge, frictional forces are generated between the steel strands and the saddle tubes on the arc segment by the tension of the cables. Due to the existence of friction, the tension of the steel strands varies along the direction of the tube.

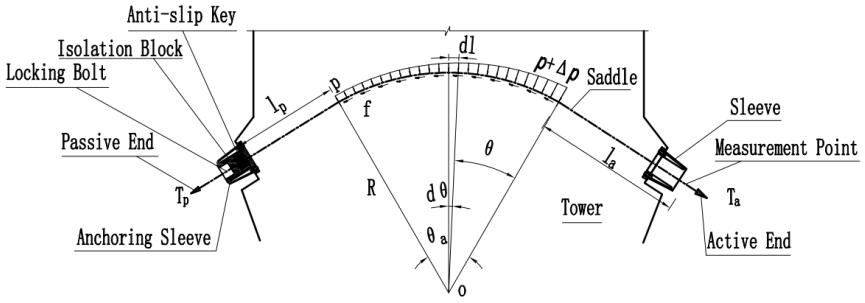

(a) Cable forces in the saddle

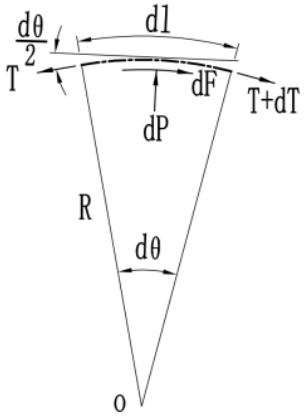

(b) Cable force elemental diagram

Fig. 6. Brief diagram of forces in a cable saddle

Taking into account the elongation of the cable during tensioning, the reverse frictional effect in the saddle arc segment can be derived from the elemental forces on the cable, as shown in Figure 6 (b).

$$dP = T\sin\frac{d\theta}{2} + (T + dT)\sin\frac{d\theta}{2} \approx Td\theta \tag{1}$$

$$dF = \mu dP \approx \mu T d\theta \tag{2}$$

From the balance of forces, it can be derived:

$$T + dT + dF = T \tag{3}$$

By combining equations (2) and (3), we can obtain:

$$\frac{dT}{T} = -\mu d\theta \tag{4}$$

By integrating and substituting the boundary condition of $\theta_a = 0$ at the active end, we can obtain:

$$\ln \frac{T}{T_a} = -\mu\theta \tag{5}$$

The tension at each point on the cable arc segment can be obtained as follows:

$$T = T_a e^{-\mu\theta} \tag{6}$$

By integrating, the elongation of the cable considering the reverse frictional effect can be obtained as follows:

$$\Delta l = \frac{T_a}{EA}\left[l_a + e^{-\mu\theta_a} l_p + \frac{R}{\mu}\left(1 - e^{-\mu\theta_a}\right) \right] \tag{7}$$

where F is the frictional force between the saddle and the cable, P is the radial pressure generated by the cable on the saddle arc surface, R is the radius of the saddle, θ_a is the central angle corresponding to the arc segment, θ is the angle of the arc between the active end of the saddle to the calculated point (in radians). T_a is the tension at the active end, l_a is the straight distance from the arc tangent point at the active end to the measurement point, l_p is the straight distance from the arc tangent point at the passive end to the anchor point, as shown in Figure 6. E is the elastic modulus of the steel strands, and A is the cross-sectional area of the cable.

The calculation should take into account the influence of the radius difference of each tube.

4.5 Analysis of Test Results

During the entire loading process of cable C23, the displacements of steel strands at each measurement point in relation to the loading process are shown in Figure 7.

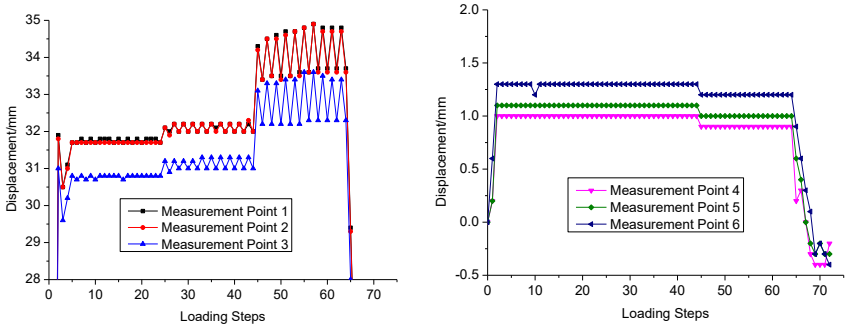

(a) Displacement of active end (b) Displacement of passive end

Fig. 7. Relationship between displacement and loading process of cable C23

Based on the loading process and Figure 7, the following observations can be made:

Under the initial cable force, the unbalanced cable forces from dead load, and unbalanced cable force from live load ($\Delta T_{23\text{-}1}$=350 kN), the displacement of the steel strands at both the active and passive ends shows a linear increase as the cable force increases, the displacement at the active end exhibits a sawtooth-like cyclic variation pattern when the live load undergoes cyclic fluctuations.

Similarly, when the unbalanced live load cable force increases to 1.4 times ($\Delta T_{23\text{-}2}$=490 kN) and 2.5 times ($\Delta T_{23\text{-}3}$=875 kN), the displacement at the active end cyclically varies with the loading and unloading process. The displacement at section 1-1 (located at the active end) is much larger than that at section 2-2 (located at the passive end), as shown in Table 1.

Table 1. Maximum displacement of measuring points on cable

Test sections	Measurement points	Cable C23 Displacememt (mm)		(②-①)/①	Cable C1 Displacememt (mm)		(④-③)/③
		Computed values①	Measured value②		Computed values③	Measured value④	
1-1	1	31.46	34.7	10.3%	34.82	34.1	-2.1%
	2	31.07	34.6	11.4%	34.18	34.8	1.8%
	3	30.42	33.4	9.8%	33.12	34.0	2.7%
2-2	4	0.96	0.9	-6.2%	1.07	1.0	-6.5%
	5	0.96	1.0	4.2%	1.07	0.8	-25.2%
	6	0.96	1.2	25.0%	1.07	1.0	-6.5%

Note: The displacement of the active end in the table is positive when it displaces to the right, while the passive end is positive when it displaces to the left, as shown in Figure 6 (a).

When the active end load is 6975 kN and the passive end load is 5500 kN, the active end displacement of C23 are 34.7, 34.6, and 33.4mm at the three measurement points, respectively. According to the authors' research, both the magnitude of cable tension and the radius of the saddle affect the coefficient of friction, the coefficient of friction is 0.162 here. So the elongation of the steel strands at each measurement point can be calculated as 31.46, 31.07, and 30.42mm in term of formula (7), the effect of the

pre-tensioned force of cable needs to be deducted. The measured values are 10.3%, 11.4% and 9.8% different from the calculated values respectively, which suggests that the displacement variation at the active end of the anchor is mainly caused by the elongation of the strands. The difference between the measured value and the calculated value is mainly caused by manufacturing and installation errors, as well as compression of anti-slip keys etc.

Meanwhile, the displacement at the passive end is 0.9, 1.0, and 1.2mm, respectively, which is close to the calculated values too. From the observed data, it can be seen that during the initial loading stage, the passive end experiences deformation due to the tightening of the anti-slip keys and elongation of the exposed steel strands. However, during the cyclic loading process, the displacement changes minimally. It can be seen that due to the resisting effect of the anti-slip keys and the friction between strands and tubes, the passive end is not very sensitive to live load changes at the active end.

In the third low cycle loading stage, when the active end load increased to 6975 kN and the load difference increased to 1475 kN, the passive end displacement decreased by 0.1mm. This indicates that with the increase of the active end tension, the friction is overcome and the cable force transfers to the passive end. So despite the tightening of the locking bolts, due to manufacturing and installation errors, there is still a slight amount of movement space for the anti-slip key within the anchoring sleeve. When there is a significant tension difference between active and passive end, the anti-slip key is tightly attached in reverse to the anchor steel plate of the saddle, resulting in a displacement reduction at the measurement points. This suggests that a small amount of force transfer occurs through the anti-slip anchorage device from the active end to the passive end.

From the cable forces test results, it can be observed that the passive end force starts to show a slight increase in the third loading stage, with a total incremental force ΔT_P of 5 kN and a force transfer rate $\Delta T_P / \Delta T_{23\text{-}4}$ of 0.3%. This indicates that the amount of force transferred through the anti-slip anchorage device is very small, suggesting minimal slippage between the anti-slip keys and the steel strands.

In the entire loading process of the anti-slip test of the cable C1, the relationship between steel strands displacement and load is shown in Figure 8.

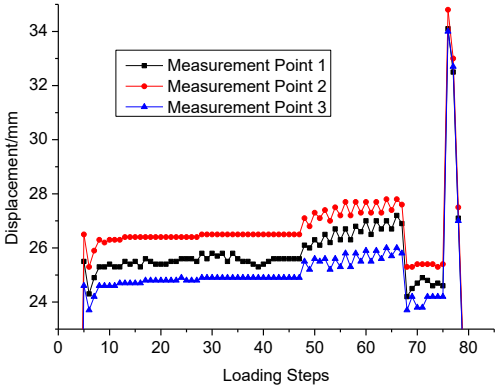

(a) Displacement of active end

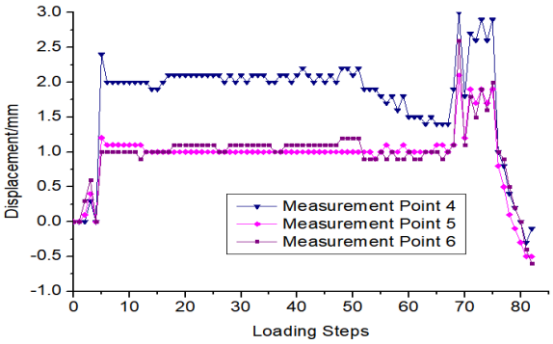

(b) Displacement of passive end

Fig. 8. Relationship between displacement and loading process of cable C1

From Figure 8, it can be observed that the displacement of the cable C1 during the loading process follows a similar pattern to cable C23. The displacements at the active end are 34.1, 34.8, and 34.0mm at the three measurement points respectively, when the tension at the active end is 7200 kN (close to the maximum load capacity of the jack) and the tension at the passive end is 4700 kN , as shown in Table 1. The coefficient of friction is 0.117 here, so the steel strands elongation calculated are 34.82, 34.18, and 33.12mm respectively, the measured values are -2.1%, 1.8% and 2.7% different from the calculated values. It indicates the same conclusion as the cable C23.

During the three-stage loading process, there is only a small variation in displacement at measuring points 5 and 6 at the passive end, but measuring point 4 has a larger displacement than points 5 and 6, and a significant reduction is observed, when the tension increases to 5750kN at active end, as shown in figure 8. When the tension at the active end reaches 7200 kN and the tension difference was 2500 kN, the decrease in displacement is even bigger. This indicates that with the increase of the active end tension, the friction is overcome and the cable force transfers to the passive end too. Although the cable force is considerable, there are no signs of the cable saddle anchoring device being pulled apart or damaged.

As long as the installation process ensures proper fitting of the anti-slip key and there is virtually no relative sliding between the anti-slip key and the steel strand, the anti-slip key can effectively function. In this case, the tension from the active end cannot be transmitted to the passive end through the anti-slip key. Similarly, the reverse action is also true. The presence of the anti-slip key acts as a barrier to the transfer of tension.

During the reverse loading process, the displacement of each measurement point at the active end decreases by 2.1 to 2.7mm. meanwhile the displacement of the measurement points at the passive end significantly increases, and it exceeds the calculated values by a significant amount. This indicates that there is some movement space for the anti-slip key of the strands in the anchorage sleeve, which is mainly caused by manufacturing and installation errors, and there is minimal deformation in the anchorage sleeve and its bolt connection with the tower.

Overall, the anchorage device exhibits effective anti-slip capabilities under both forward and reverse giant loading.

5 Conclusion

The model experiment, which focused on two cables of different angle, was conducted on the anti-slip performance of the saddle under low-cycle repeated loading, simulating operational load conditions. This study represents the largest-scale experiments of its kind conducted in the word. The main research focused on the anti-slip performance under unbalanced cable forces during operation, reverse anti-slip capability, cable force transmission ratio, and ultimate anti-slip load-bearing capacity. The main conclusions obtained from the experiment are as follows:

(1) From the measured data, it can be observed that under the same applied load, the displacement values at different measurement points of the cables are almost equal, indicating uniform stress distribution among the steel strands. Under unbalanced cable forces, the displacement at the passive end is much smaller than that at the active end. The displacement transducers return to 0 after unloading, indicating that the cables remain in the elastic stage throughout the test and no anti-slip failure occurs.

(2) Due to manufacturing and installation errors, there is a certain amount of movement space for the steel strands' anti-slip keys. However, its influence is limited. In the C23 cable test, the unbalanced cable force at the active end resulted in an additional 5 kN at the passive end, with a cable force transmission ratio of 0.3%. The passive end of the C1 cable did not show a significant increase in passive cable force, indicating that the anti-slip anchorage device effectively controls the minimal transfer of cable force across the saddle.

(3) A calculation formula considering reverse frictional effect for cable elongation is derived. It shows that the displacement variation at the cable saddle is mainly caused by the cable elongation. The difference between the measured value and the calculated value is mainly caused by manufacturing and installation errors, as well as compression of anti-slip keys.

(4) It can be seen that due to the resisting effect of the anti-slip keys and the friction between strands and tubes, the passive end is not very sensitive to live load changes at the active end. But with the increase of the active end tension, the friction is overcame and the cable force transfers to the passive end.

(5) There is a slight amount of movement space for the anti-slip keys in the anchorage sleeve due to manufacturing and installation errors, but virtually no sliding occurs between the anti-slip keys and the steel strands, so it does not affect their engineering application.

(6) The cable loading test with the active and passive ends swapped showed that the anchorage device has effective bidirectional anti-slip capability for the cables. The ultimate anti-slip capacity test demonstrated that the anti-slip device still has reliable anti-slip performance when subjected to a maximum load of 7200 kN and an unbalanced load of 2500 kN.

Based on the above experiments, it can be concluded that the anti-slip anchorage device provides effective anchoring for the steel strands of the cables at the saddle.

References

1. David Collings, BSc, CEng, FICE, et al. (2013) Extradosed and cable-stayed bridges, exploring the boundaries. 166(4) , 231-239.
2. Akio Kasuga.(2006)Extradosed Bridges in Japan, Structural Concrete 7(3):91-103.
3. TANG Shao-qing, CAI Wen-sheng, WANG Jie-zao, WANG Shuang-yan. (2002) Section Model Test Research in Saddles of Zhangzhou War Preparation Bridge. Bridge Construction, 1, 15-18,32.
4. GUAN Run-rong, ZHANG Jun-ping, LIU Ai-rong, ZHOU Ming-yuan. (2005) Segment model test research on saddles of partially cable-stayed bridge. Journal of Guangzhou University(Natural Science Edition) ,5, 449-453.
5. SONG Mao-lin. (2008) The Test Method of Cable Tower Full Size Model for Pony Cable-Stayed Bridge. SHANXI SCIENCE & TECHNOLOGY of COMMUNICATIONS, 2, 59-61,84.
6. LIU Zhao, MENG Shaoping, ZANG Hua, ZHANG Yufeng. (2007) Model test and design investigation on saddle deviator zone of extra-dosed bridge. JOURNAL OF SOUTHEAST UNIVERSITY(NaturalScience Edition), 2, 291-295.
7. YANG Xiao-yan. (2011) Model Test for Stay Cable Saddle Zone of Shawan Bridge in Guangzhou. Bridge Construction, 3, 31-35.
8. LI Wen-xian, SONG Qiang, QIN Wei-wei, WEI Fu-tang, QIU Min LI Hua-ping, ZHONG Yi. (2012) Development and Application Of Device Of Crisscross Slip Resistant Studs for Extradosed Bridge. Bridge Construction, 42(06), 92-97.
9. ZOU Kaicheng, HUANG Qunhui. (2016) Anti-slipping Test of Unilateral Bidirectional Anchoring Device in the Extradosed Cable-stayed Bridge. Transportation Science &Technology, 1, 27-30.
10. Xu Qifeng, Yang Xiaohai, Jiang Ping, You Xiaoxiang, Gu Zhan, Wang Fei. (2019) Experimental Study on the Saddle of Diamond Split Tubes of Extradosed Cable-stayed Bridge. Highway, 64(02), 160-163.
11. REN Wan-min, REN Jie, YUAN Ming, ZHU Min. (2019) Key Techniques of Design of Extradosed Cable-Stayed Bridge on Chengdu-Kunming Railway. Bridge Construction, 49(01), 95-100.
12. Extra-Dosing Girder Bridges in India Sub Continent, (2010) 3rd International fib Congress, Think Globally & Build Locally, Washington.
13. Jan Biliszczuk, Jerzy Onysyk, Wojciech Barcik, et al. (2017) Extradosed Bridges in Poland-Design and Construction. Frontiers in Built Environment,2, 1-9.
14. Bishal Agarwal1, Dr. Vijay Raj, Anand Kumar Singh, Susanta Kumar Sethy, (2019) Review Paper on Economical Design of Extra dosed Bridge on a Highway. International Journal of Research in Advent Technology, 7(3),1080-1084.
15. FU Xiao-fan, CHEN Chu-long. (2021) Bridge Type Selection for Main Bridge of Third Yili River Bridge. Bridge Construction, 53(S1), 119-126.
16. YU Zheng. (2021) Study on Key Construction Technology of Cable-Stayed Bridge with High Piers and Multiple Spans Crossing Wangjiahe River. Journal of China & Foreign Highway, 41(3), 110-115.

17. LI J, YANG D Y, HU Y L, et al. (2022)Full-Scale Model Experimental Study of the HDPE Multitube Saddle of an Extradosed Bridge [J]. Structural Engineering International, 32(4), 527-537.